ORIGINAL RESEARCH

Investigations into the Adsorption Isotherm and Kinetics of Heavy Metal Removal Using Green Iron Oxide Nanoparticles

Article History
Received: 01-Jan-2024
Revised: 05-Feb-2025
Accepted: 05-Mar-2025
Published: 16-Mar-2025

Kirti Srivastava[a]*, Roli Verma[a], R.S.Jagadish[a], Yamini Pandey[a], Abhishek Kumar[a]

Abstract: Iron oxide nanoparticles (IONPs) are highly effective and environmentally sustainable adsorbents for the removal of heavy metals from wastewater. This study focuses on exploring a green route for synthesizing IONPs using *Hibiscus rosa-sinensis* petal extract, promoting an eco-friendly approach. The synthesized particles were evaluated analytically using XRD, confirming a crystallite size of 6.16 nm, and were assessed for adsorption of Pb(II) and Cu(II) ions. Optimized adsorption conditions, including pH 5 and an interaction period of 30 minutes, resulted in high removal efficiencies of 95.48% for Pb(II) and 84.9% for Cu(II). Adsorption behavior was best explained by the Langmuir isotherm, revealing maximum adsorption capacities of 30.77 mg/g and 28.74 mg/g for Pb(II) and Cu(II) respectively, while kinetic studies confirmed a pseudo-second-order model. These findings underscore the potency of green-synthesized IONPs as a promising and sustainable solution for wastewater treatment, paving the way for their potential real-world applications.
Keywords: Green iron oxide nanoparticles, Heavy metals, Adsorption, Chemical kinetics, Isotherm

INTRODUCTION

When discharged into natural water bodies, industrial effluent containing heavy metals poses serious risks to the health of people, animals, and plants. Heavy metals are persistent in soil and water and have been associated with severe health issues, including cancer. For example, lead exposure is linked to anemia and high blood pressure, while excessive copper can damage the liver, kidneys, heart, and brain. Recognizing these risks, the U.S. Environmental Protection Agency (EPA) has defined regulatory limits in drinking water for copper and lead at 1.3 mg/L and 0.015 mg/L, respectively. These concerns highlight the urgent need to remove Pb^{2+} and Cu^{2+} from aquatic environments (USEPA, 2007).

Conventional methods, such as evaporation, chemical precipitation, electroplating, ion exchange, and membrane processes, have been used to mitigate heavy metal contamination in wastewater (Fu, F. et al., 2011; BIS, 2012; Wang et al., 2009; Singh et al., 2019; Eyvaz et al., 2022). However, these techniques often fall short due to high costs and inefficiency at low metal concentrations. Adsorption has emerged as a cost-effective and selective alternative, utilizing materials like activated carbons (Deliyann et al., 2015), clay minerals (Gu, S. et al., 2019), chelating agents (Sabaté Reboll, J. et al., 2016), and chitosan/natural zeolites (Irannajad, M. et al., 2021), biological species (Srivastava, K. et al., 2022). Despite their promise, traditional

a Department of Chemistry, JSS Academy of Technical Education, Sector 62, Noida, India
* **Corresponding Author's Email:** kisrivast@gmail.com

adsorbents face limitations, necessitating the exploration of innovative and affordable alternatives with superior performance.

Low-cost adsorbents derived from industrial waste by-products, including fly ash (Al-Zboon, K. et al., 2011; Wang, S. et al., 2007), blast furnace sludge (Srivastava, S. K. et al., 1997), waste slurry (Namasivayam, C. et al., 1995), lignin (Carrott, P. J. M. et al., 2007), $Fe(OH)_3$ (Namasivayam, C. et al., 1998) and red mud waste slurry (Gupta, V. K. et al., 2002; Almeida, A. C. M. et al., 2021) as well as agricultural residues like sawdust (Semerjian, L. (2018), areca waste (Subramani, B. S. et al., 2019), and tea factory waste (Nuhoğlu, Y. et al., 2021), and battery industry waste (Zhang, Y. et al., 2020) have been studied for heavy metal removal. While these materials are affordable and abundant, challenges such as scalability, activation wastewater management, and limited efficiency have hindered their widespread application (Irannajad et al., 2021).

Nanomaterials have demonstrated remarkable promise for the removal of heavy metals, especially nanoscale zero-valent iron (NZVI) and FeO_4 (magnetite) nanoparticles. NZVI offers high surface area, reduced chemical requirements, and faster reaction rates, though it faces challenges like particle aggregation (Chen, S. Y. et al., 2008; Thirunavukkarasu, A. et al., 2020; Srivastava, K. et al., 2021). Magnetite nanoparticles, with their large surface area (Da Costa et al., 1994; Singh et al., 2017) and superparamagnetic properties (Sivashankar, R. et al., 2014), enable efficient heavy metal removal and easy separation using an external magnetic field. They are non-toxic, environmentally friendly, reusable, and maintain high efficacy after multiple regeneration cycles (Zargoosh, K. et al., 2013; Prasad, C. et al., 2017; Venkateswarlu, S. et al., 2014).

Green synthesis of iron nanoparticles, using biological systems such as plant extracts, inactivated plant tissue, exudates, and other components of live plants offers improved stability and environmental compatibility (Sugumaran, M. et al., 2012; Latha et al., 2014; Shojaee, S. et al., 2016; Gupta, K. et al., 2021; Nizamuddin, S. et al., 2019; Arora, R., 2019). *Hibiscus rosa-sinensis*, a widely known ornamental plant rich in bioactive compounds like flavonoids, tannins, and phenolics, has been identified as an excellent source for green synthesis. Its petal extracts provide an eco-friendly route to synthesize iron oxide nanoparticles with enhanced properties [42].

In this study, iron oxide nanoparticles have been synthesized using *Hibiscus rosa-sinensis* petal extracts through a green approach. These nanoparticles have been characterized using advanced analytical techniques, and their nanoscale structure has been confirmed. Their efficacy in removing Pb^{2+} and Cu^{2+} from wastewater has been evaluated under varying conditions of adsorbent dose, pH, and contact time. The adsorption behavior has been analyzed using Freundlich and Langmuir isotherm models, and additional kinetic studies have provided insights into the rate of adsorption. The potential of green-synthesized iron oxide nanoparticles as an effective, economical, and ecologically friendly method of eliminating heavy metals from aquatic ecosystems has been highlighted by this thorough study.

MATERIALS AND METHODS

Preparation of Extract

Flowers from hibiscus plants were collected. Flowers were stripped of their stamens and calices, then their petals were dried in the shade and ground into a fine powder using a blender. The prepared powder was stored at 4 °C in an airtight container for future use. 5 g of hibiscus petal powder was mixed with 100 mL of distilled water in an Erlenmeyer flask and the mixture was then heated at 60 °C for 1 hr. The mixture was then filtered using Whatman filter paper No. 1 and the filtrate was centrifuged for 15 minutes at 6000 rpm to take out tiny fragments. This extract served as the reducing agent for the synthesis of nanoparticles.

Synthesis of Iron Nanoparticles

Iron chloride hexahydrate ($FeCl_3 \cdot 6H_2O$, analytical grade) supplied by Sigma-Aldrich (Sigma-Aldrich 220299) served as the precursor. 100 cc of distilled water was used to dissolve .027 g of iron chloride hexahydrate $FeCl_3 \cdot 6H_2O$ for preparing a solution of 1 mM concentration. The extract of Hibiscus rosasinensis flower was mixed in 1:1 ratio with 1 mm $FeCl_3 \cdot 6H_2O$ in an Erlenmeyer flask to synthesize iron nanoparticles. For an optimized reaction, the solution was thoroughly mixed at 250 rpm for an hour at room temperature. The solution was centrifuged at 6000 rpm for 15 minutes once the precipitate became visible. To get rid of all contaminants, the precipitate was rinsed with water and centrifuged in the same circumstances. To eliminate moisture and undesirable particles, the resultant pellet was

 https://doi.org/10.37819/nanofab.10.2050

overnight heated in a hot air oven at 48°C. A muffle furnace set to 405°C for 3 hours and was used to calcine the dried nanoparticle powder. For additional characterization and application research, nanoparticles were gathered and stored in a vial.

MATERIALS AND METHODS

Preparation of Extract

Flowers from hibiscus plants have been collected. The stamens and calices have been stripped from the flowers, and their petals have been dried in the shade and ground into a fine powder with the help of a blender. The powdered petals have been stored in an airtight container at 4° C for future use and examination. A mixture comprising 5 g of hibiscus petal powder and 100 mL of distilled water has been prepared in an Erlenmeyer flask and subjected to heating at 60° C for one hour. After the mixture has been filtered using Whatman filter paper No. 1, the filtrate has been centrifuged for 15 minutes at 6000 rpm to remove tiny fragments. This extract has been used as a reducing agent for the synthesis of nanoparticles.

Synthesis of Iron Nanoparticles

Iron chloride hexahydrate ($FeCl_3 \cdot 6H_2O$), of high purity and analytical grade, has been utilized and purchased from Sigma-Aldrich (Sigma-Aldrich 220299). A 1 mm $FeCl_3 \cdot 6H_2O$ solution has been prepared by dissolving 0.027 g of iron chloride hexahydrate in 100 cc of distilled water. This solution has been mixed in a 1:1 ratio with the extract of Hibiscus rosa-sinensis flowers in an Erlenmeyer flask for synthesizing iron nanoparticles. To optimize the reaction, the solution was thoroughly mixed at 250 rpm for one hour at room temperature. Once a precipitate has been formed, the solution has been centrifuged at 6000 rpm for 15 minutes. The precipitate has been rinsed with water and centrifuged under the same conditions to eliminate contaminants.

To remove moisture and undesirable particles, the resultant pellet has been heated overnight in a hot air oven at 48° C. The dried nanoparticle powder has been calcined in a muffle furnace set to 405° C for 3 hours. The synthesized nanoparticles have been collected and stored for future use.

NANOPARTICLE CHARACTERIZATION

UV-VIS Spectrophotometry (Model: G10S, Thermo Fisher Scientific Ltd., USA) has been employed for the initial confirmation of the synthesized Fe_3O_4 nanoparticles. The sample has been scanned to determine its absorbance maxima at wavelengths in the range of 200 to 700 nm.

The nature of the adsorbents on nanoparticles has been investigated using FTIR spectroscopy. An FTIR spectroscope has been employed to scan the samples at wavelengths between 8000 and 300 cm^{-1}, displaying the results as a spectrum. The procedure involved mixing 150 mg of KBr and 0.5 mg of the sample.

An X-ray diffractometer (Xpert Pro, Belgium) has been used to assess the crystalline size of the nanoparticles. Using Debye-Scherrer's equation, the size has been determined from the spectrum:

$$D = \frac{K * \lambda}{\beta \cos\theta} \quad (1)$$

D: particle size
K: form factor
λ: wavelength
θ: Bragg's angle
β: full width at half maximum

BATCH TESTS FOR SOLUTIONS WITH A SINGLE METAL ION

Stock solutions of $Pb(NO_3)_2$ and $CuSO_4$ with a strength of 1000 mg/L have been prepared in distilled water. The solutions have been diluted as required, and analyses have been performed. The analytical-grade chemicals have been purchased from Sigma-Aldrich.

BATCH TESTS FOR SOLUTIONS WITH A SINGLE METAL ION

25.0 mL of Pb(II) and/or Cu(II) solution with an initial concentration ranging from 30 to 70 mg/L were diluted 50 mL using distilled water. Adsorption isotherms were determined by introducing 0.05 g iron oxide nanoparticles to respective 25.0 ml of metal ion solution. The pH of the solution has been adjusted to 5 ± 0.2. Samples have been collected at regular intervals of 5 minutes from 5–40 minutes. During all

kinetic studies, the samples were vigorously shaken for 60 minutes at 200 rpm. After each time interval, the suspensions have been filtered through Whatman filter paper No. 42, and the quantity of heavy metals in the filtrate has been determined using an atomic absorption spectrophotometer.

The effect of pH has also been studied with the same value of metal ion solution and adsorbent. pH adjustments have been made using either 1M HCl or 1M NaOH.

ANALYSIS OF EXPERIMENTAL DATA

Kinetic Model

Adsorption kinetics is a crucial factor in evaluating the effectiveness of the sorption process, as it defines the rate at which solutes are adsorbed and the residence time of adsorbates at the solid-liquid interface. The rate at which adsorption occurs is dependent on the number of particles adhering to the adsorbent surface per second and the frequency of particle collisions per unit area per second.

The impact of time on the sorption process is examined to determine the kinetic behavior of adsorbates on adsorbents. In this study, pseudo-first-order and pseudo-second-order kinetic models have been used to analyze the impact of contact time on Pb and Cu adsorption by iron oxide nanoparticles. Adsorption data for adsorbates extracted from aqueous solutions are frequently analyzed using the pseudo-first-order model. According to this concept, the number of vacant binding sites on the adsorbent surface closely correlates with the adsorption rate.

Conversely, the pseudo-second-order kinetic model concentrates on adsorption processes that are controlled by interactions between adsorbates and the functional groups on the surface of the adsorbent that are mediated by chemical bonds. Based on equilibrium adsorption, this model takes into account that the amount of adsorbate adsorbed at equilibrium and the amount adsorbed at a specific time both influence the adsorption rate (Ho, Y. S., & McKay, G., 2000; Singh, S. et al., 2021).

The linear equation of pseudo-first-order kinetic equation is given below:

$$\ln(q_e - q_t) = \ln q_e - k_1 t \quad (2)$$

In eq. (2)

q_e = amount adsorbed by nanoparticle at equilibrium by Pb and Cu in (mg/g),

q_t = amount adsorbed at time t in (mg/g),

k_1 = rate constant of first-order kinetics/minute.

q_e, k_1 and R^2 were determined by straight line plots of log $(q_e - q_t)$ against time.

The kinetic rate equation of pseudo-second-order kinetics is given by equation 3:

$$\frac{t}{q_t} = \frac{1}{k_2 q_e^2} + \frac{t}{q_e} \quad (3)$$

In eq. (3)

k_2 = rate constant of pseudo-second-order kinetics (mg/g/min),

k_2, q_e, and R^2 values were determined from the slope and intercept of the plots of t/q_t against time.

Analysis of Pb(II) and Cu(II) adsorption

The eq. (4) and (5) are used to determine the amounts of Pb(II) and Cu(II) adsorbed by iron oxide nanoparticles:

$$q = \frac{V\,(C_o - C_e)}{W} \quad (4)$$

$$\%\,\text{Removal} = \frac{(C_o - C_e) \times 100}{C_o} \quad (5)$$

C_e = concentration of metal ions at equilibrium in (mg/L),

V = volume of solution of metal (L),

W = mass of the adsorbent (g), and

q = quantity of metal ions absorbed by iron oxide nanoparticles (mg/g). Experiments were carried out at room temperature.

Adsorption isotherm

Among the various adsorption isotherms, Langmuir and Freundlich's isotherms are widely preferred for describing adsorption data across a broad spectrum of adsorbate concentrations. Langmuir adsorption isotherm assumes that homogeneous monolayer adsorption occurs at all surface sites, preventing interactions between adsorbed molecules and molecules at nearby adsorption sites (Ho & McKay, 2000).

Langmuir equation in linear form is given below.

$$\frac{C_e}{q_e} = \frac{1}{(b * q_{max})} + \frac{1}{q_{max}} * C_e \quad (6)$$

 https://doi.org/10.37819/nanofab.10.2050

In eq. (6),

q_e = Amount of adsorbed metal ions in (mg/g),
C_e = Concentration at equilibrium in (mg/L).
q_{max} = Maximum adsorption,
b = Chemical affinity between adsorbent and adsorbate.

Freundlich isotherm equation is as follows:

$$q_e = K_F * C^{1/n} \quad (7)$$

Eq. (5) in the logarithmic form is as follows

$$\text{Log}q_e = \text{Log}K_F + \frac{1}{n}\text{Log}C_e \quad (8)$$

$1/n$ and K_F are isotherm constants respectively.

RESULTS AND DISCUSSION

Nanoparticle Characterization

UV-Visible Spectroscopy

A typical transformation of the extract solution's color of the solution of the extract from pinkish violet to black when the solution of iron salt was added to Hibiscus rosasinensis flower extract, served as preliminary confirmation for the generation of iron oxide nanoparticles (Latha, N. et al., 2014, Niraimathee, V. A. et al., 2016). The absorbance spectra of the solution were measured across the wavelength range of 200 to 1000 nm. **Fig. 1** displays the UV-VIS absorption spectra of the produced iron oxide. The highest absorbance was detected at 229 nm, with no peaks observed at 590 nm and 300 nm. These wavelengths correspond to the presence of various natural compounds in the extract. This suggests that during the synthesis of Fe_3O_4 nanoparticles, the hibiscus extract functions as both a reducing and capping agent.

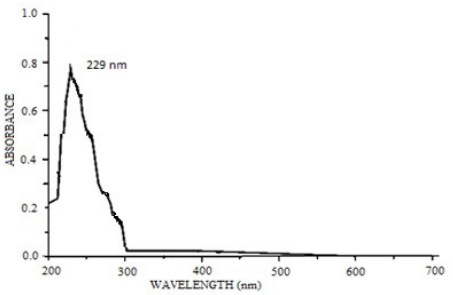

Figure 1. UV-VIS spectrum of Iron Oxide nanoparticle.

FTIR Spectroscopy

FTIR analysis was carried out for IONPs and hibiscus extract to check for any possible modifications to the bonds between functional group atoms that might have happened during the process of reduction.

Fig. 2(a) shows the FTIR spectrum of *Hibiscus rosa-sinensis* extracts, while **Fig. 2(b)** depicts the FTIR spectrum of iron oxide nanoparticles synthesized using the same extract. Significant bands were observed at 1630 cm^{-1} and 3396 cm^{-1}, corresponding to O–H bending and O–H stretching vibrations, respectively (Niraimathee, V. A. et al., 2016). These bands are primarily from the presence of water molecules in the sample. Additionally, multiple peaks corresponding to various organic functional groups were identified: C–H stretching at 2396 cm^{-1}, C=C stretching at 1630 cm^{-1}, and C–O–C bending and stretching at 1412 cm^{-1} and 1062 cm^{-1}, respectively. These peaks confirm the presence of flavonoids, terpenoids, tannins, and organic acids in the flower extract (Niraimathee, et al., 2016 Lesiak et al., 2019).

In the case of the nanoparticles, the presence of Fe is evident from the prominent broad peak at 567.95 cm^{-1} and an intense peak at 460 cm^{-1}, corresponding to the tetrahedral stretching and octahedral bending vibrations of Fe–O–Fe, respectively (Lesiak et al., 2019). These findings align with the UV-visible spectra discussed earlier and confirm the successful synthesis of the nanoparticles. It was found that the intensity of absorption bands was higher than that of the extract. It confirms the reducing action of the extract in the formation of iron oxide nanoparticles.

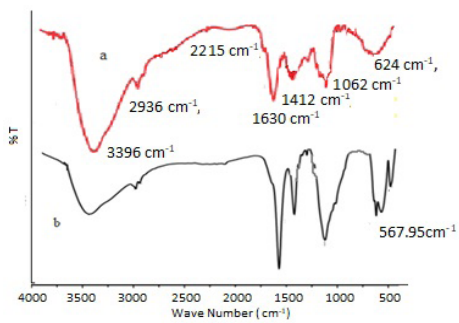

Figure 2. a. FTIR spectrum of Hibiscus Extract **b.** FTIR spectrum of Iron oxide nanoparticle.

XRD Analysis

To further ensure the formation of nanoparticles, XRD was conducted to determine the crystalline phases and crystallite size of the synthesized nanoparticles. By applying the Scherrer constant of 0.9 and utilizing the Debye-Scherrer equation, the average crystallite size was determined as 6.16 nm. The XRD pattern of the synthesized nanoparticles, shown in **Fig. 3**, exhibits multiple diffraction peaks corresponding to Fe_3O_4 at 2θ values of 29.2°, 35.4°, 43.1°, 53.4°, 57°, and 62.6°. These peaks correspond to the (220), (311), (400), (422), (511), and (440) Bragg reflection planes, respectively, as per JCPDS card 65-3107 (Shi et al., 2015).

These reflections confirm the formation of Fe_3O_4 nanoparticles. The presence of additional peaks may be attributed to residual impurities from the plant extract. However, these results are completely following the existing literature on Fe_3O_4 nanoparticles, which consistently report Fe_3O_4 diffraction planes within the 2θ range of 30°–60° (Hou, C. L. et al., 2013).

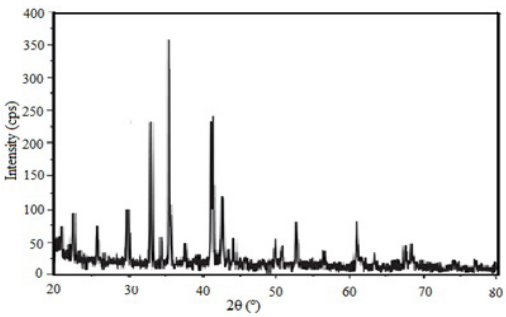

Figure 3. XRD image of iron oxide nanoparticle.

Role of Contact Time

The impact of time on removal on Pb (II) and Cu(II) was studied at different time intervals as shown in **Fig. 4**. Both Pb and Cu ions show a sharp increase in percentage removal within the first 5 minutes, achieving 82.86% removal for Pb and 76.9% removal for Cu, indicating rapid adsorption at the beginning of the process. After 10 minutes, the rate of removal slows down, and the curves plateau, suggesting that equilibrium has been reached. The maximum percentage removal is achieved within 30 minutes, with Pb (II) reaching 95.48% and Cu (II) reaching 84.9%. This can be a result of the adsorbent initially having a large surface area (physical adsorption). When the pores present over the adsorbent surface got clogged with heavy metal ions due to saturation on the binding site, the rate started to decrease towards a steady state. In this investigation, the contact time adsorption curve revealed three adsorption phases: the initial phase, which saw rapid heavy metal ion adsorption; the 2nd phase, which saw gradual slowing of the adsorption rate; and the equilibrium phase, which showed no discernible change in removal rate (Ho, Y. S. et al., 2000).

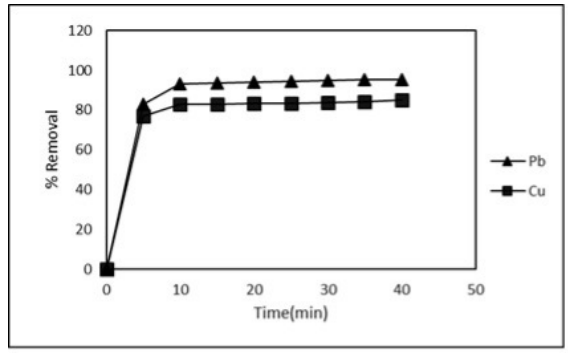

Figure 4. Effect of Contact Time on % Removal of Heavy metal ions.

Effect of pH

Several studies indicate that pH is a very important factor in determining the adsorption of heavy metals. The binding between the adsorbent and metal ions is often attributed to surface charges, functional groups, adsorbent solubility, and the degree of ionization. From **Fig. 5**, it was observed the removal efficiency for both Pb (II) and Cu (II) increases proportionally with an increase of pH from 1 to 4, indicating that adsorption is favored at high pH value. At lower pH values (below 2), adsorption is relatively low, likely due to the high concentration of hydrogen ions (H^+) competing with metal ions for adsorption sites. Pb (II) achieves maximum removal efficiency at a pH of approximately 5, with a removal percentage exceeding 95%. Similarly, Cu (II) reaches its maximum removal efficiency at a pH range of 4–5, with a removal percentage of about 85%.

Beyond pH 5–6, a slight decline in removal efficiency is observed for both metals, possibly due to the formation of metal hydroxides or precipitation at higher pH levels, which reduces the availability of free metal ions for adsorption. The optimal pH range for the effective removal of Pb (II) and Cu (II) is between 4 and 5. Consequently, pH 5 is selected as the optimum value for adsorption experiments. This

 https://doi.org/10.37819/nanofab.10.2050

finding emphasizes the importance of pH in optimizing adsorption processes for the removal of heavy metals from aqueous solutions.

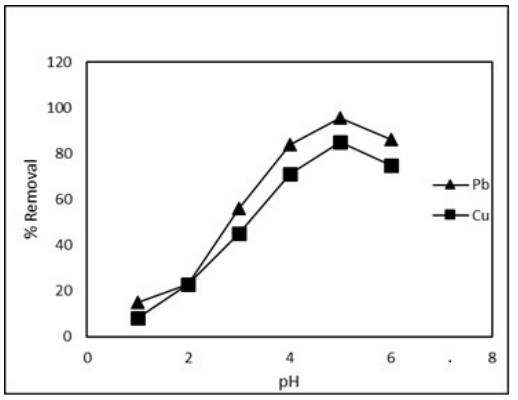

Figure 5. Effect of pH on % Removal of Heavy metal.

Dose of Adsorbent

The percentage removal of Cu (II) and Pb (II) ions as a function of adsorbent dosage is shown in **Fig. 6**. The removal efficiency of both metals increases with adsorbent dosage, peaking at 40–50 mg, which can be attributed to higher number of adsorption sites available. Pb (II) achieves a maximum removal efficiency of 95%, while Cu (II) reaches 84.9%, indicating a stronger adsorption affinity of Pb (II) for the adsorbent. Beyond 40–50 mg, the removal efficiency stabilizes, suggesting adsorption site saturation, where excess adsorbent does not significantly enhance removal. Based on this trend, 50 mg is considered the optimal adsorbent dose Additionally, Pb (II) consistently exhibits higher removal efficiency than Cu (II) at all doses, likely due to stronger bonding interactions between Pb (II) ions and the functional groups on the surface of iron oxide nanoparticles.

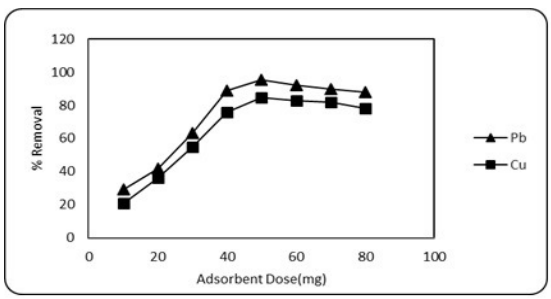

Figure 6. Effect of adsorbent doses on % Removal

Kinetic Model Analysis

The kinetic model elucidates the mechanisms and reaction pathways governing the adsorption of Pb(II) and Cu(II) over IONPs. It is possible to analyze the adsorption rate, describe the process efficiently, and identify the kind of adsorbent-adsorbate interactions—differentiating between physisorption and chemisorption—by fitting experimental data to several kinetic models. The adsorption kinetics are analyzed using both pseudo-first-order and pseudo-second-order models, as shown in **Fig. 7** and **8**.

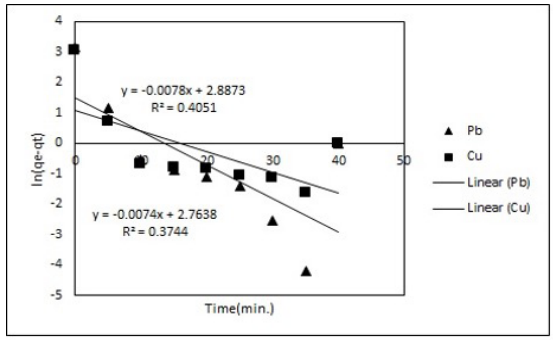

Figure 7. Pseudo-first order plot for Heavy metal ion removal at different time intervals

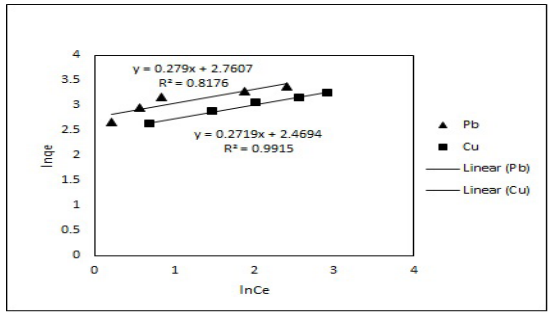

Figure 8. Pseudo-second order plot for Heavy metal ion removal at different time intervals

The pseudo-second-order models fit well the adsorption data much better (R^2 = 0.9998 for both Pb(II) and Cu(II)) compared to the pseudo-first-order, which has significantly lower R^2 values (0.3744 for Pb and 0.4051 for Cu). The pseudo-first-order model, which assumes physisorption via weak van der Waals forces, does not adequately describe the adsorption process. In contrast, the pseudo-second-order model, based on chemisorption involving covalent bonding or electron sharing, provides a near-perfect fit, confirming that

chemisorption governs the adsorption mechanism. The pseudo-second-order rate constant (k_2) is significantly higher than the pseudo-first-order rate constant (k_1), further supporting the dominance of chemisorption. Additionally, the pseudo-second-order model predicts higher equilibrium adsorption capacities (q_e) of 24.04 mg/g for Pb(II) and 21.23 mg/g for Cu(II) compared to the pseudo-first-order model (q_e = 15.86 mg/g for Pb(II) and 17.94 mg/g for Cu(II)). This confirms that the pseudo-second-order model more accurately represents the actual adsorption capacity. **Table 1** summarizes the kinetic parameters for Pb(II) and Cu(II) adsorption onto iron oxide nanoparticles.

Table 1. Kinetic Parameters for pseudo-first and pseudo-second-order model.

		Metal Ions	
Kinetic Model	**Constants**	**Pb**	**Cu**
Pseudo-first order	k_1	0.0074	0.0078
	q_e	15.86	17.94
	R_2	0.3744	0.4051
Pseudo-second order	k_2	0.1081	0.1541
	q_e	24.04	21.23
	R_2	0.9998	0.9998

Adsorption Isotherm Model Analysis

Table 2 displays the Freundlich and Langmuir adsorption parameters, which were obtained from Langmuir isotherm (**Fig. 9**) and Freundlich isotherm (**Fig. 10**). **Fig. 10** shows that Pb has a lower slope (0.0325) than Cu (0.0348), indicating that Pb has a slightly higher adsorption capacity. The maximum adsorption capacities of the nanoparticles for Pb and Cu were determined to be 30.77 mg/g and 28.74 mg/g, respectively. Additionally, Pb exhibits a higher Langmuir constant (b = 0.9503 L/mg) compared to Cu (b = 0.3997 L/mg), suggesting stronger adsorption affinity. The Freundlich model fits Cu adsorption very well (R^2 = 0.9915) but does not fit Pb adsorption as well (R^2 = 0.8176). The adsorption intensity values (n) for both Pb (3.58) and Cu (3.68) are greater than 1, indicating favorable adsorption and an increase in adsorption strength with concentration. Pb also has a higher Freundlich constant (K_F = 15.81 mg/g) than Cu (K_F = 11.81 mg/g), suggesting greater adsorption capacity in a heterogeneous system.

Table 2. Adsorption Parameters & Constant of Langmuir and Freundlich adsorption isotherm models

		Metal ions	
Adsorption Isotherm Model	**Constants**	**Pb**	**Cu**
Langmuir	Q_{max}	30.77	28.74
	b	0.9503	0.3997
	R^2	0.9972	0.9973
Freundlich	K_F	15.81	11.81
	n	3.584	3.6778
	R^2	0.8176	0.9915

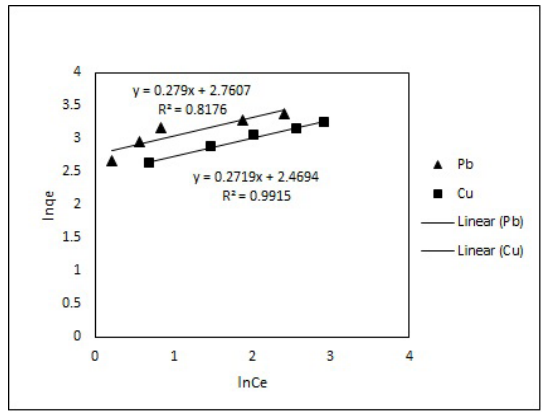

Figure 9. Langmuir Isotherm for Heavy metal ion removal at various concentrations

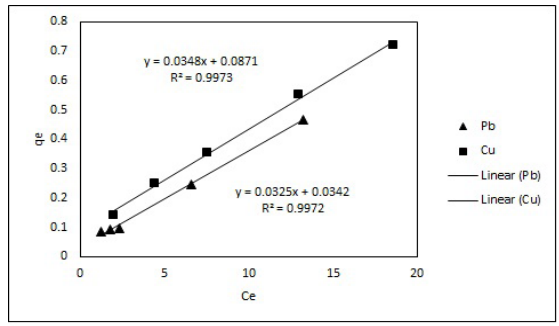

Figure 10. Freundlich Isotherm for Heavy metal ion removal at various concentrations

Overall, the Langmuir model provides a better fit for Pb adsorption (R^2 = 0.9972 vs. 0.8176 for Freundlich), indicating that Pb adsorption is primarily monolayer. In contrast, the Freundlich model fits Cu adsorption well (R^2 = 0.9915), though the Langmuir fit is also strong (R^2 = 0.9973), suggesting

 https://doi.org/10.37819/nanofab.10.2050

that Cu adsorption may involve both monolayer and multilayer mechanisms. The iron oxide nanoparticles are more effective for Pb adsorption than for Cu, as Pb exhibits higher adsorption capacity and stronger affinity.

CONCLUSIONS

This study investigates the adsorption of Pb(II) and Cu(II) ions using iron oxide nanoparticles, focusing on adsorption kinetics, isotherms, pH dependence, and adsorbent dosage. Adsorption occurs rapidly, with over 80% removal within 5 minutes and equilibrium reached in 30 minutes. Maximum removal efficiencies are 95.48% for Pb(II) and 84.9% for Cu(II), following a pseudo-second-order kinetic model, indicating chemisorption.

Adsorption efficiency peaks at pH 5 for Pb(II) (95%) and pH 4–5 for Cu(II) (85%), decreasing at lower pH due to H^+ competition and slightly declining beyond pH 5 due to metal hydroxide precipitation. Increasing adsorbent dosage enhances removal, stabilizing beyond 40–50 mg due to site saturation. Pb(II) consistently shows a stronger adsorption affinity than Cu(II). Isotherm analysis identifies the Langmuir model as the best fit, with maximum adsorption capacities of 30.77 mg/g for Pb(II) and 28.74 mg/g for Cu(II).

The study highlights the cost-effectiveness and scalability of iron oxide nanoparticles for wastewater treatment, supporting global sustainability efforts. However, its focus on Pb(II) and Cu(II) limits applicability to real-world wastewater systems with multiple contaminants. Key challenges include varying environmental conditions, competitive adsorption, regeneration potential, and industrial scalability. Future research should explore these factors to enhance the long-term viability of iron oxide nanoparticles for wastewater treatment.

REFERENCES

Almeida, A. C. M., do Nascimento, R. A., Amador, I. C. B., de Sousa Santos, T. C., Martelli, M. C., de Faria, L. J. G., & da Paixão Ribeiro, N. F. (2021). Chemically activated red mud: assessing structural modifications and optimizing adsorption properties for hexavalent chromium. *Colloids and Surfaces A: Physicochemical and Engineering Aspects*, *628*, 127325.

Al-Zboon, K., Al-Harahsheh, M. S., & Hani, F. B. (2011). Fly ash-based geopolymer for Pb removal from aqueous solution. *Journal of hazardous materials*, *188*(1-3), 414–421.

Arora, R. (2019). Adsorption of heavy metals–a review. *Materials Today: Proceedings*, *18*, 4745–4750.

Carrott, P. J. M., & Carrott, M. R. (2007). Lignin–from natural adsorbent to activated carbon: a review. *Bioresource technology*, *98*(12), 2301–2312.

Chen, S. Y., Chen, W. H., & Shih, C. J. (2008). Heavy metal removal from wastewater using zero-valent iron nanoparticles. *Water Science and Technology*, *58*(10), 1947–1954.

Da Costa, G. M., De Grave, E., De Bakker, P. M. A., & Vandenberghe, R. E. (1994). Synthesis and characterization of some iron oxides by sol-gel method. *Journal of Solid State Chemistry*, *113*(2), 405–412.

Deliyanni, E. A., Kyzas, G. Z., Triantafyllidis, K. S., & Matis, K. A. (2015). Activated carbons for the removal of heavy metal ions: A systematic review of recent literature focused on lead and arsenic ions. *Open Chemistry*, *13*(1), 000010151520150087.

Drinking water standard and health advisories table, SanFrancisco; United States Environmental ProtectionAgency (USEPA), 2007.

Eyvaz, M., Albahnasawi, A., Gürbulak, E., & Yüksel, E. (Eds.). (2022). *Water Conservation: Inevitable Strategy*. BoD–Books on Demand.

Fu, F., & Wang, Q. (2011). Removal of heavy metal ions from wastewaters: a review. *Journal of environmental management*, 92(3), 407–418.

Gu, S., Kang, X., Wang, L., Lichtfouse, E., & Wang, C. (2019). Clay mineral adsorbents for heavy metal removal from wastewater: a review. *Environmental Chemistry Letters*, *17*, 629–654.

Gupta, K., Joshi, P., Gusain, R., & Khatri, O. P. (2021). Recent advances in adsorptive removal of heavy metal and metalloid ions by metal oxide-based nanomaterials. *Coordination Chemistry Reviews*, *445*, 214100.

Gupta, V. K., & Sharma, S. (2002). Removal of cadmium and zinc from aqueous solutions using red mud. *Environmental Science & Technology*, *36*(16), 3612–3617.

Ho, Y. S., & McKay, G. (2000). The kinetics of sorption of divalent metal ions onto sphagnum moss peat. *Water research*, *34*(3), 735–742.

Hou, C. L., Li, T. H., Zhao, T. K., Liu, H. G., Liu, L. H., & Zhang, W. J. (2013). Electromagnetic

wave absorbing properties of multi-wall carbon nanotube/Fe_3O_4 hybrid materials. *New Carbon Materials*, *28*(3), 184–190. In: Drioli, E., Giorno, L. (eds) Encyclopedia of Membranes. Springer, Berlin, Heidelberg.

Indian standard drinking water specifications, (2nd Eds.), New Delhi, India; Bureau of India Standards (BIS), 2012.

Irannajad, M., & Kamran Haghighi, H. (2021). Removal of heavy metals from polluted solutions by zeolitic adsorbents: a review. *Environmental Processes*, *8*, 7–35.

Latha, N., & Gowri, M. (2014). Biosynthesis and characterisation of Fe_3O_4 nanoparticles using Caricaya papaya leaves extract. *Int J Sci Res*, *3*(11), 1551–1556.

Lesiak, B., Rangam, N., Jiricek, P., Gordeev, I., Tóth, J., Kövér, L., ... & Borowicz, P. (2019). Surface study of Fe_3O_4 nanoparticles functionalized with biocompatible adsorbed molecules. *Frontiers in chemistry*, *7*, 642.

Namasivayam, C., & Ranganathan, K. (1998). Effect of organic ligands on the removal of Pb (II), Ni (II) and Cd (II) by 'waste' Fe (III)/Cr (III) hydroxide. *Water Research*, *32*(3), 969–971.

Namasivayam, C., & Yamuna, R. T. (1995). Waste biogas residual slurry as an adsorbent for the removal of Pb (II) from aqueous solution and radiator manufacturing industry wastewater. *Bioresource Technology*, *52*(2), 125–131.

Niraimathee, V. A., Subha, V., Ravindran, R. E., & Renganathan, S. (2016). Green synthesis of iron oxide nanoparticles from Mimosa pudica root extract. *International Journal of Environment and Sustainable Development*, *15*(3), 227–240.

Nizamuddin, S., Siddiqui, M. T. H., Mubarak, N. M., Baloch, H. A., Abdullah, E. C., Mazari, S. A., ... & Tanksale, A. (2019). Iron oxide nanomaterials for the removal of heavy metals and dyes from wastewater. *Nanoscale materials in water purification*, 447–472.

Nuhoğlu, Y., Ekmekyapar Kul, Z., Kul, S., Nuhoğlu, Ç., & Ekmekyapar Torun, F. (2021). Pb (II) biosorption from the aqueous solutions by raw and modified tea factory waste (TFW). *International Journal of Environmental Science and Technology*, 1–12.

Prasad, C., Karlapudi, S., Rao, C. N., Venkateswarlu, P., & Bahadur, I. (2017). A highly resourceful magnetically separable magnetic nanoparticles from aqueous peel extract of Bottle gourds for organic dyes degradation. *Journal of Molecular Liquids*, *243*, 611–615.

Sabaté Reboll, J. (2016). Heavy metal recovery by chelating agents and membranes.

Semerjian, L. (2018). Removal of heavy metals (Cu, Pb) from aqueous solutions using pine (Pinus halepensis) sawdust: Equilibrium, kinetic, and thermodynamic studies. *Environmental technology & innovation*, *12*, 91–103.

Shi, D., Yang, H., Ji, S., Jiang, S., Liu, X., & Zhang, D. (2015). Preparation and characterization of core-shell structure Fe_3O_4@ C magnetic nanoparticles. *Procedia engineering*, *102*, 1555–1562.

Shojaee, S., & Shahri, M. M. (2016). Green synthesis and characterization of iron oxide magnetic nanoparticles using Shanghai white tea (Camelia sinensis) aqueous extract.

Singh, A. K., Srivastava, O. N., & Singh, K. (2017). Shape and size-dependent magnetic properties of Fe_3O_4 nanoparticles synthesized using piperidine. *Nanoscale research letters*, *12*, 1–7.

Singh, S., Kapoor, D., Khasnabis, S., Singh, J., & Ramamurthy, P. C. (2021). Mechanism and kinetics of adsorption and removal of heavy metals from wastewater using nanomaterials. *Environmental Chemistry Letters*, *19*(3), 2351–2381.

Singh, S., Kumar, V., Romero, R., Sharma, K., & Singh, J. (2019). Applications of nanoparticles in wastewater treatment. *Nanobiotechnology in bioformulations*, 395–418.

Sivashankar, R., Sathya, A. B., Vasantharaj, K., & Sivasubramanian, V. (2014). Magnetic composite an environmental super adsorbent for dye sequestration–A review. *Environmental Nanotechnology, Monitoring & Management*, *1*, 36–49.

Srivastava, K., Srivastava, A., Singh, P., & Sharma, V. (2021). Remediation of distillery waste water using zero valent iron nanoparticles. *Current Research in Green and Sustainable Chemistry*, *4*, 100072.

Srivastava, K., Srivastava, A., & Singh, P. (2022). Kinetic and Adsorption Isotherm studies for the removal of Heavy Metals by Rhizoclonium Species. RJPBCS,13,4,56-63. https://doi.org/10.33887/rjpbcs/2022.13.4.1

Srivastava, S. K., Gupta, V. K., & Mohan, D. (1997). Removal of lead and chromium by activated slag—a blast-furnace waste. *Journal of Environmental Engineering*, *123*(5), 461–468.

Subramani, B. S., Shrihari, S., Manu, B., & Babunarayan, K. S. (2019). Evaluation of pyrolyzed areca husk as a potential adsorbent for the removal of Fe2+ ions from aqueous solutions. *Journal of environmental management*, *246*, 345–354.

Sugumaran, M., Poornima, M., & Sethuvani, S. (2012). Phytochemical and trace element analysis of Hibiscus rosa sinensis Linn and Hibiscus syriacus Linn flowers. *NPAIJ*, *8*(9), 341–345.

Thirunavukkarasu, A., Nithya, R., & Sivashankar, R. (2020). A review on the role of nanomaterials in the removal of organic pollutants from wastewater. *Reviews in Environmental Science and Bio/Technology*, *19*(4), 751–778.

Venkateswarlu, S., Kumar, B. N., Prasad, C. H., Venkateswarlu, P., & Jyothi, N. V. V. (2014). Bio-inspired green synthesis of Fe_3O_4 spherical magnetic nanoparticles using Syzygium cumini seed extract. *Physica B: Condensed Matter*, *449*, 67–71.

Wang, S., Li, L., & Zhu, Z. H. (2007). Solid-state conversion of fly ash to effective adsorbents for Cu removal from wastewater. *Journal of hazardous materials*, *139*(2), 254–259.

Wang, X., Zheng, Y., & Wang, A. (2009). Fast removal of copper ions from aqueous solution by chitosan-g-poly (acrylic acid)/attapulgite composites. *Journal of Hazardous Materials*, *168*(2-3), 970–977.

Zargoosh, K., Abedini, H., Abdolmaleki, A., & Molavian, M. R. (2013). Effective removal of heavy metal ions from industrial wastes using thiosalicylhydrazide-modified magnetic nanoparticles. *Industrial & Engineering Chemistry Research*, *52*(42), 14944–14954.

Zhang, Y., Wang, Y., Zhang, H., Li, Y., Zhang, Z., & Zhang, W. (2020). Recycling spent lithium-ion battery as adsorbents to remove aqueous heavy metals: Adsorption kinetics, isotherms, and regeneration assessment. *Resources, Conservation and Recycling*, *156*, 104688.